

Preparation and tensile properties of Al₂O₃/Ni-Co nanocomposites

WANG Guo-feng, JIANG Shao-song, LU Zhen, ZHANG Kai-feng

School of Materials Science and Engineering, Harbin Institute of Technology, Harbin 150001, China

Received 10 May 2011; accepted 25 July 2011

Abstract: Al₂O₃/Ni-Co composites with different additives and Al₂O₃ particles were fabricated by pulse current electrodeposition. The effects of different additives and Al₂O₃ particles on the surface smoothness, micro-hardness and plastic deformation at room temperature and high temperature were compared. Scanning electron microscopy was employed to examine the microstructures of the as-deposited and deformed samples. The hardness, fracture strength at room temperature and elongation at superplastic temperature of the material reach HV469, 1 150 MPa and 632%, respectively, when the saccharin was used as additive.

Key words: additives; composites; mechanical properties; pulse current electrodeposition

1 Introduction

Compared with the coarse-grained materials, the nanocrystalline materials possess unique physical and mechanical properties and are among the most interesting topic in the materials research [1–2]. Nanocrystalline materials can be fabricated using a top-down approach, such as severe plastic deformation (SPD), or a bottom-up approach, such as electrodeposition [3]. Pulse electrodeposition is one of the most effective methods in reducing the grain size into the nanometer range [4]. It is not only a simple and low cost technique to obtain nanocrystalline materials, but can also produce nanocrystalline materials of full density. Nanocrystalline Ni produced by electrodeposition is used as a model to study deformation [5]. Heating is a necessary condition for the plastic forming of nanocrystalline Ni since its limited ductility at room temperature. However, even at low temperatures, microstructure instability is significant since the high driving force for grain growth in nanocrystalline material [6–7]. Nanosized particle and alloying element can refine matrix microstructure and nail the grain boundary.

Ni-Co alloy and composites possess good adhesion, mechanical properties, tribological properties, corrosion resistance and thermal stability with excellent magnetic properties [8–9]. WANG and CHAN [10] reported the low-temperature superplasticity of Si₃N₄/Ni-Co nanocomposites. A maximum elongation of 692% was

obtained at a temperature of 723 K, and the nanoparticles were found to play an important role in the stability of the microstructure. The influence of particle size on the structure and tribological properties of Ni-Co composites was reported [11]. However, comparisons between the superplastic behaviors of nanocomposites containing ceramic particles with various sizes are scarce.

Al₂O₃/Ni-Co nanocomposites with different additives and Al₂O₃ particles were fabricated by pulse current electrodeposition, and their mechanical properties were investigated, with a specific emphasis on clarifying the role of additive. The microstructure evolution and the effect of particle size on the deformation behaviors were discussed.

2 Experimental

Al₂O₃/Ni-Co nanocomposites with various particle sizes of Al₂O₃ were prepared by pulse current electrodeposition. Nickel sulfamate-based electrolyte was used. The plating baths contained 350 mL/L nickel sulfamate, 2 g/L cobalt sulfamate, 15 g/L nickel chloride and 30 g/L boric acid. In order to obtain a fine grain size, 1 g/L of saccharin and 0.1 g/L of 1, 4-butyndiol were used, respectively.

The sketch map of the experimental apparatus is shown in Fig. 1. Square waves with a duty cycle of 50% were used during pulse electrodeposition. A nickel plate with a purity of 99.98% was used as an anode and stainless steel plate was used as a cathode. In order to

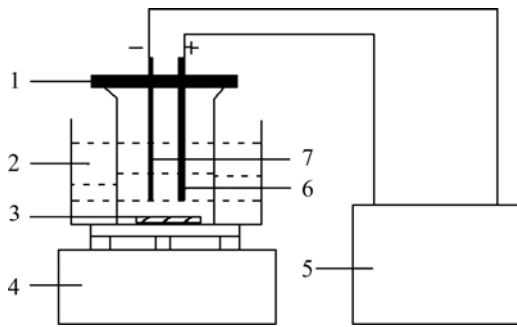


Fig. 1 Schematic diagram of electrodeposition system: 1—Locating plate; 2—Constant temperature bath with electrical heater control unit; 3—Stirring bar; 4—Magnetic stirring device; 5—Current control and power supply unit; 6—Ni plate; 7—Stainless steel plate

avoid electroplating both sides of the steel plate, one side away from the Ni plate was coated with silicon rubber. Al_2O_3 particles with mean diameter of 20, 50 and 100 nm were used. Particle agglomeration was prevented by suspending the Al_2O_3 particles in the electrolyte, and subjecting them to magnetic stirring for 16 h and ultrasonic treatment for 30 min just prior to electrodeposition. The stirring rate was kept at 500 r/min. The bath temperature was kept at (323 ± 1) K. A plating time of 6.5 h was maintained to obtain plate with a thickness of (100 ± 2) μm .

After deposition, the electrodeposits were stripped from the cathode substrate. Dog bone-shaped tensile samples were machined with a wire electrical discharge to obtain a gauge length of 10 mm and a gauge width of 3 mm. The tensile tests were conducted on an Instron 5565 test machine equipped with a ceramic heating furnace. The test temperatures were controlled within an accuracy of ± 2 K. For tensile test at high temperature, samples were placed in the furnace at the specified test temperature for about 20 min to establish thermal equilibrium. All of the tests were conducted in air at various strain rates and deformation temperatures. Transmission electron microscopy (TEM) was performed on a Jeol 2010 operated at 200 kV. The microstructures of the samples were observed by scanning electron microscopy (SEM). Electron backscatter diffraction (EBSD) measurements were performed on the deformed sample on an FEI Quanta 200 FEG scanning electron microscope equipped with a TSL OIM system.

3 Results and discussion

TEM images of the electrodeposited $\text{Al}_2\text{O}_3/\text{Ni-Co}$ nanocomposites with different additives are shown in Fig. 2. It is obvious that saccharin is better than 1, 4-butyne diol to obtain a fine grain. The mean grain size of the deposited material with additive of 1, 4-butyne diol

and saccharin are 180 and 37 nm, respectively. The diffraction pattern of the selected area shown in the inset in Fig. 2(b) is ring pattern, which also illustrates the ultrafine-grained structure. In Fig. 2(b), a circular pore is also found. The pore may be formed by the loss of Al_2O_3 particle during the preparation of samples.

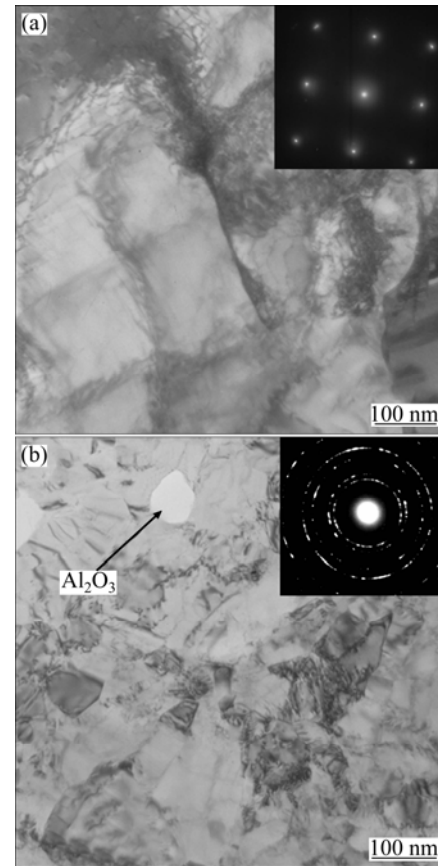


Fig. 2 Bright field TEM images showing deposited microstructures with different additives: (a) 1, 4-butyne diol; (b) Saccharin

The effect of Al_2O_3 content on the microhardness of the deposited materials with different additives is shown in Fig. 3. For comparison, the microhardness of the deposited materials without additive was measured too. It is seen from the figure that adding additives results in its hardening by the grain refinement mechanism. The microhardness of the deposited materials without additive is HV270 when the Al_2O_3 content is 0.35% and increases to HV360 and HV420 with using additive of 1, 4-butyne diol and saccharin, respectively. The increase of microhardness was observed on the incorporation of Al_2O_3 nanoparticles. Similar result was reported by several researchers [12]. The increase of microhardness is due to the dispersion strengthening caused by the nanoparticles. The highest microhardness of the deposited materials is HV469 when the Al_2O_3 content is 0.55% and the additive is saccharin.

Figure 4 shows the tensile behavior of $\text{Al}_2\text{O}_3/\text{Ni-Co}$

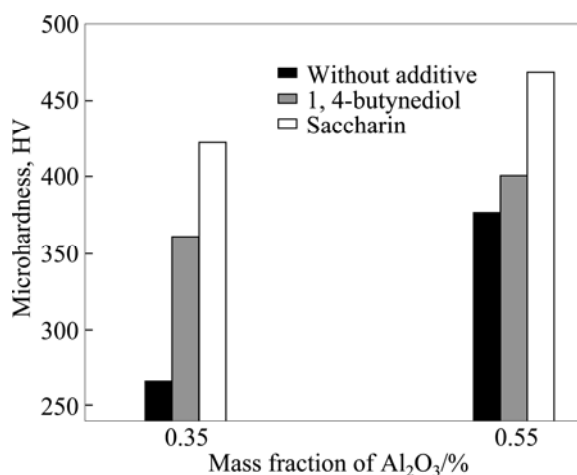


Fig. 3 Effect of Al₂O₃ mass fraction on microhardness of deposited materials with different additives

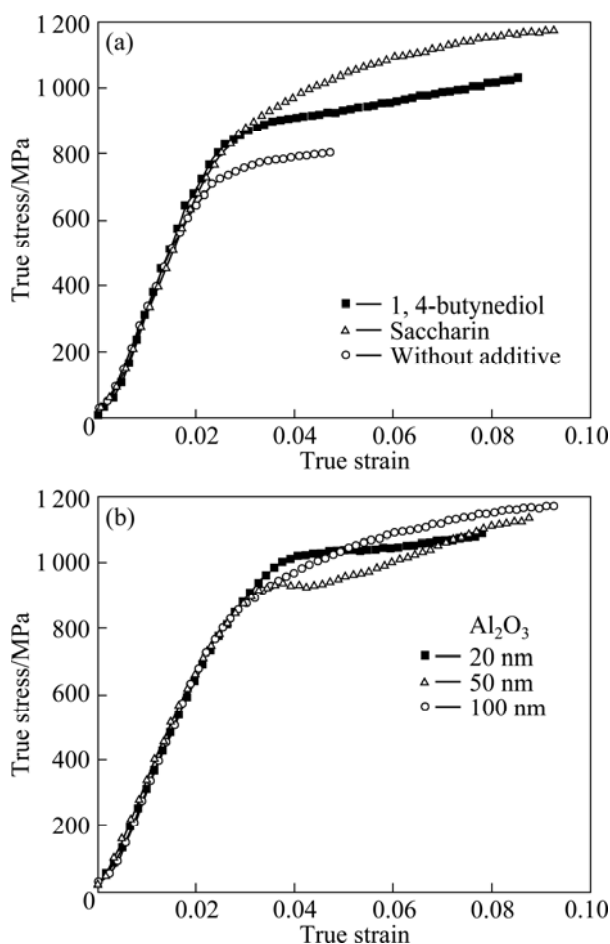


Fig. 4 Tensile stress—true strain curves of Al₂O₃/Ni-Co composites at room temperature with different additives (a) and Al₂O₃ particle sizes (b)

nanocomposites at room temperature with different additives and different Al₂O₃ particle sizes. The largest tensile elongation of the composites is 9% with adding saccharin. The tensile yield strength of the composites without additive is about 700 MPa, which is lower than

that of both composites with 1, 4-butynediol (900 MPa) and with saccharin (910 MPa). The increase of tensile strength comes from the grain size refinement. The influence of Al₂O₃ particle size on the tensile behavior of the deposited composites is shown in Fig. 4(b). With the increase of the Al₂O₃ particle size, the yield strength decreases slightly, but the strain hardening just is opposite. The largest tensile strength of 1 150 MPa is obtained with the particle size of 50 nm. The tensile specimen after fracture is also shown in Fig. 4(b). There is no apparent macroscopic necking in the gauge and the macro-fracture is shear with an angle of 60°.

Figure 5 shows the morphologies of the fracture surface of the tensile specimens. For the as-deposited materials with additive of 1, 4-butynediol, the fracture is featured by a ductile dimple-pattern with some local cleavages, which is consistent with its poor plasticity. In comparison, cleavage can hardly be seen in all the as-deposited materials with additive of saccharin. The fracture is featured by a ductile dimple-pattern. As shown in Fig. 5(c), the as-deposited material with Al₂O₃ particle size of 50 nm has a finer dimple structure than that of materials with particle sizes of 20 and 100 nm, which is consistent with its best plasticity.

Elevated temperature tension tests were performed at different temperatures. The relationship between the total elongation-to-failure and test temperatures is shown in Fig. 6. The additives and the deformation temperature show significant influence on the elongation of the deposited materials. The deposited material with additive of saccharin evidently has the highest superplasticity and that with additive of 1, 4-butynediol has no superplasticity. The largest elongation of 632% is achieved at the deformation temperature of 823 K and at a strain rate of $1.67 \times 10^{-3} \text{ s}^{-1}$. Notably, the deformation temperature in the test is almost 100 K, lower than the conventional temperature requirement of $0.5T_m$ (where T_m is the melting point of the superplastic materials).

Microstructural examination was conducted on the deposited material with additive of saccharin, which was deformed at 823 K and $1.67 \times 10^{-3} \text{ s}^{-1}$ to failure with an elongation of 632%. The microstructures and the inverse pole figure maps of the deformed sample at the grip region and the gauge region are shown in Fig. 7. Differences in the two regions are observed, although they were exposed to the same test temperature and heating time. The grains grow to a micrometer range, and the equiaxed shape is retained in the grip region. However, in the gauge region, grain sections on the RD-TD plane are elongated along the RD direction (the tension direction shown in Fig. 7(b)), while grains on the fracture surface remain approximately equiaxed, as shown in Fig. 7(c). The grains elongated in the tensile direction seem to have no preferred orientation. Larger

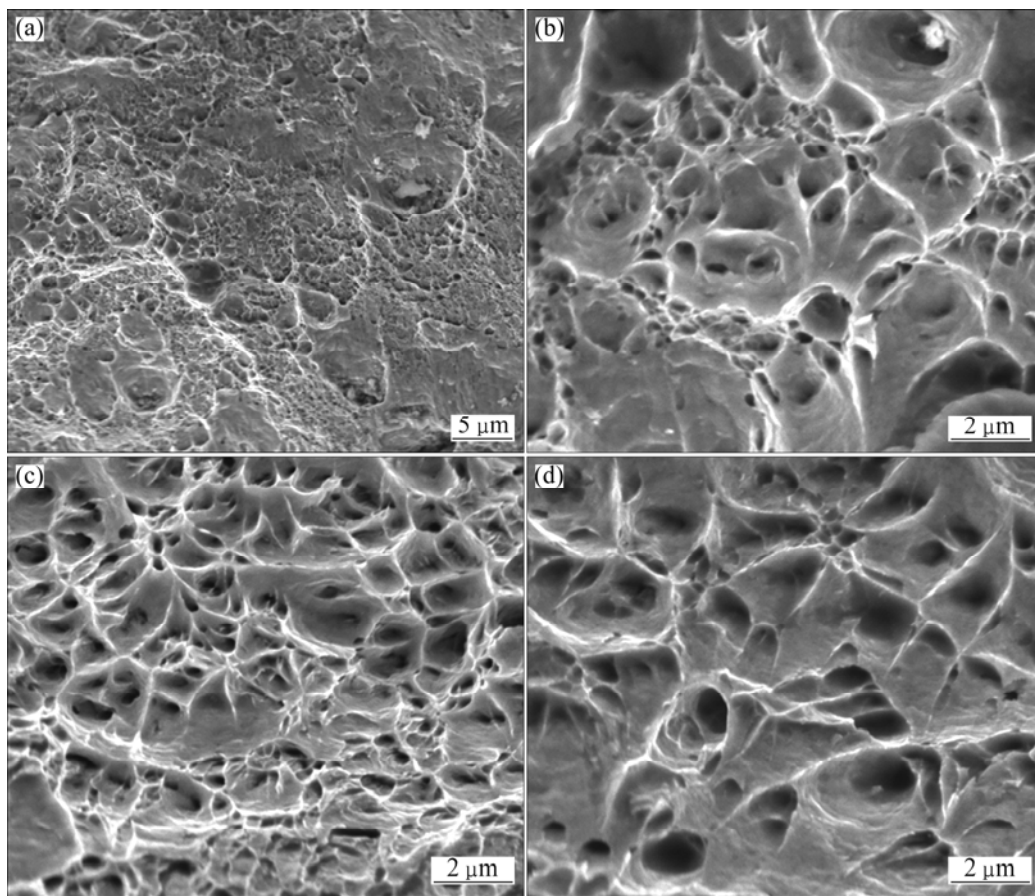


Fig. 5 Morphologies of fractured specimens of $\text{Al}_2\text{O}_3/\text{Ni-Co}$ composites with different additives and Al_2O_3 particle sizes: (a) 1, 4-butynediol, Al_2O_3 particle size of 50 nm; (b) Saccharin, Al_2O_3 particle size of 20 nm; (c) Saccharin, Al_2O_3 particle size of 50 nm; (d) Saccharin, Al_2O_3 particle size of 100 nm

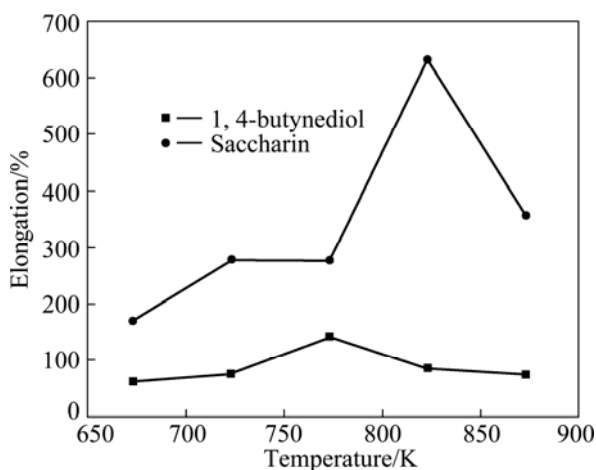


Fig. 6 Variation of elongation as function of temperature of $\text{Al}_2\text{O}_3/\text{Ni-Co}$ composites with different additives

grain size is observed in the gauge region of Ni-Co alloy, which was reported in Ref. [6]. By comparing the grain size of the two regions, it can be seen that the dynamic grain growth is much greater than the static grain growth. The formation of the elongated grains is related to the diffusion creep behavior [13] and dislocation slip [14]. It

should be remembered that deformation with the dislocation slip tends to form some preferred crystallographic orientation. On the other hand, the diffusional flow has no relation to the preferred orientation formation. Therefore, change in crystallographic orientation during superplastic deformation probably gives significant information on the superplastic mechanism [15]. Grain boundary character distribution (GBCD), which influences grain boundary sliding as a main mechanism of superplasticity, was also examined as fractions of low-angle (L), coincidence site lattice (Σ) and random (R) boundaries. The difference in fraction of low angle boundaries should be noted. The fraction in the grip region is 3.5%, which increases up to 5.7% in the gauge region. This means that the superplasticity of the deposited material is accommodated by dislocation glide mechanism, at least partially.

4 Conclusions

1) The $\text{Al}_2\text{O}_3/\text{Ni-Co}$ composites with the additive of saccharin have finer microstructure and better

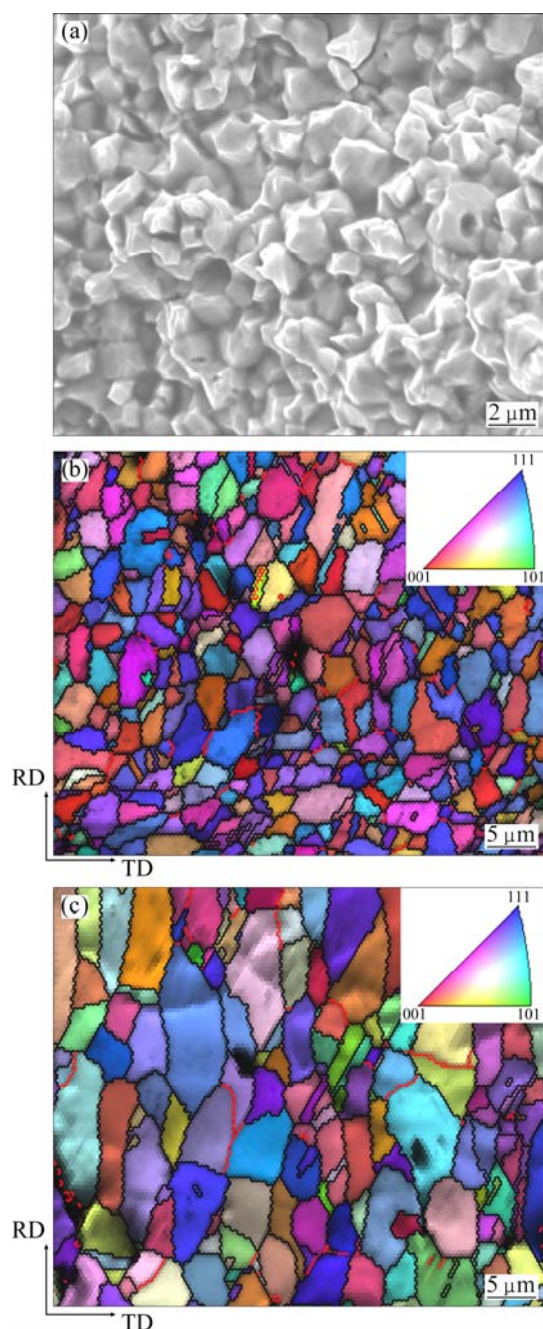


Fig. 7 Microstructure of gauge region (a) and inverse pole figure maps of tensile specimen deformed at 823 K and $1.67 \times 10^{-3} \text{ s}^{-1}$ in grip and gauge regions (b, c): (a) Fracture surface of gauge region; (b) Grain boundary of L of 3.5%, Σ of 35.4% and R of 61.1%; (c) Vertical tensile axis, grain boundary of L of 5.7%, Σ of 36.7% and R of 57.6% (L is red lines, Σ and R are black lines)

mechanical properties than those with the additive of 1, 4-butyne diol. The grain size of Ni matrix and the micro-hardness reach 37 nm and HV469, respectively.

2) The tension tests were carried out at room temperature. The tension strength of 1 150 MPa and elongation of 9% are obtained. The fracture is featured by a ductile dimple-pattern.

3) The $\text{Al}_2\text{O}_3/\text{Ni-Co}$ composites with the additive of saccharin exhibit low-temperature superplasticity with a maximum elongation of 632% at a temperature of 823 K and at a strain rate of $1.67 \times 10^{-3} \text{ s}^{-1}$. The grain is elongated along the tensile direction during superplastic deformation. Dislocation glide is the dominant superplastic accommodation process.

References

- [1] RAJGARHIA R K, SPEAROT D E, SAXENA A. Behavior of dopant modified interfaces in metallic nanocrystalline materials [J]. *JOM*, 2010, 62(12): 70–74.
- [2] GLEITER H. Nanostructured materials: basic concepts and microstructure [J]. *Acta Materialia*, 2000, 48(1): 1–28.
- [3] MEYERS M A, MISHRA A, BENSON D J. Mechanical properties of nanocrystalline materials [J]. *Prog Mater Sci*, 2006, 51: 427–556.
- [4] PADMANABHAN K A. Grain boundary sliding controlled flow and its relevance to superplasticity in metals, alloys, ceramics and intermetallics and strain-rate dependent flow in nanostructured materials [J]. *J Mater Sci*, 2009, 44: 2226–2238.
- [5] PRASAD M J N V, CHOKSHI A H. Superplasticity in electrodeposited nanocrystalline nickel [J]. *Acta Materialia*, 2010, 58: 5724–5736.
- [6] WANG G F, CHAN K C, ZHANG K F. Low temperature superplasticity of nanocrystalline electrodeposited Ni-Co alloy [J]. *Scripta Mater*, 2006, 54: 765–769.
- [7] CHAN K C, WANG G F, WANG C L, ZHANG K F. Low temperature and high strain rate superplasticity of the electrodeposited Ni/ Si_3N_4 (w) composite [J]. *Scripta Material*, 2005, 53: 1285–1290.
- [8] QIN L Y, LIAN J S, JIANG Q. Enhanced ductility of high-strength electrodeposited nanocrystalline Ni-Co alloy with fine grain size [J]. *Journal of Alloys and Compounds*, 2010, 504: 439–442.
- [9] SRIVASTAVA M, WILLIAM G, RAJAM K S. Electrodeposition of Ni-Co composites containing nano- CeO_2 and their structure, properties [J]. *Applied Surface Science*, 2010, 257: 717–722.
- [10] WANG C L, CHAN K C. Enhanced low-temperature superplasticity of Ni-Co alloy by addition of nano- Si_3N_4 particles [J]. *Materials Science and Engineering A*, 2008, 491: 266–269.
- [11] SRIVASTAVA M, WILLIAM G, JAIN A, RAJAM K S. Influence of SiC particle size on the structure and tribological properties of Ni-Co composites [J]. *Surface & Coatings Technology*, 2007, 202: 310–318.
- [12] SRIVASTAVA M, WILLIAM GRIPS V K, RAJAM K S. Electrochemical deposition and tribological behaviour of Ni and Ni-Co metal matrix composites with SiC nano particles [J]. *Applied Surface Science*, 2007, 253: 3814–3824.
- [13] SRIVASTAVA S, MCNEE K R, GREENWOOD G W, JONES H. Creep behaviour of AZ61 magnesium alloy at low stresses and intermediate temperatures [J]. *Mater Sci Technol*, 2004, 20: 42–46.
- [14] MCFADDEN S X, ZHILYAEV A P, MISHRA R S, MUKHERJEE A K. Observations of low-temperature superplasticity in electrodeposited ultrafine grained nickel [J]. *Mater Lett*, 2000, 45: 345–349.
- [15] TAKAYAMA Y, FURUSHIRO N, KIMIJIMA E, KATO H. Change in crystallographic orientation distribution during superplastic deformation in an Al-Zn-Mg-Cu alloy [J]. *Materials Science and Engineering A*, 2005, 410–411: 114–119.

$\text{Al}_2\text{O}_3/\text{Ni-Co}$ 纳米复合材料的制备与拉伸性能

王国峰, 蒋少松, 卢振, 张凯锋

哈尔滨工业大学 材料科学与工程学院, 哈尔滨 150001

摘要: 采用脉冲电沉积制备了含有不同添加剂和不同 Al_2O_3 颗粒的 $\text{Al}_2\text{O}_3/\text{Ni-Co}$ 复合材料, 比较了不同添加剂和不同 Al_2O_3 颗粒对材料表面光洁度、显微硬度、室温和高温下的塑性变形, 采用扫描电子显微镜观察变形前、后材料的微观组织。当采用糖精为添加剂时, 材料的硬度、室温断裂强度、超塑温度下的延伸率分别达到 469HV、1 150 MPa 和 632%。

关键词: 添加剂; 复合材料; 力学性能; 脉冲电沉积

(Edited by LI Yan-hong)